The 2015 World Congress on
Advances in Structural Engineering and Mechanics (ASEM15)
Incheon, Korea, August 25-29, 2015

Temperature-effect compensation for prestress-loss monitoring in PSC girders using mountable PZT interface

Thanh-Canh Huynh[1)], Kwang-Suk Lee[1)] Tuan-Cuong Nguyen[1)], and *Jeong-Tae Kim[2)]

[1), 2)] *Department of Ocean Engineering, Pukyong National University, Busan, Korea*
[2)] idis@pknu.ac.kr

ABSTRACT

This study has been motived to monitor the prestress force in prestressed concrete (PSC) girders by estimating the effect of temperature variation. Firstly, an impedance-based technique using mountable PZT interface is proposed for prestress-loss monitoring in tendon-anchorage of PSC girders. A cross correlation-based algorithm using an effective frequency shift (EFS) of impedance signatures is visited to estimate the temperature-effect. Secondly, lab-scale experiments are performed on a PSC girder instrumented with a mountable PZT interface at tendon-anchorage. A series of temperature variation and prestress-loss events are simulated for the PSC girder. Thirdly, the feasibility of the mountable PZT interface for prestress force monitoring is experimentally verified for the prestress-loss scenarios under constant temperatures. Finally, the applicability of the temperature-effect compensation technique using the EFS is examined for the prestress-loss monitoring in PSC girders under temperature variation.

1. INTRODUCTION

Damage monitoring in structural systems by using local impedance properties has been studied by many researchers. The impedance-based method was first proposed by Liang et al. (1994). As the local dynamic characteristics, the method utilizes electro-mechanical (EM) impedance of a coupled PZT (Lead Zirconate Titanate) -structure system to detect the incipient change in structural characteristics at local critical region. Recently, the impedance-based method has been applied for monitoring prestress-loss in PSC bridges by detecting the change in impedance responses at the tendon-anchorage connection (Kim et al. 2006, Kim et al. 2010, Nguyen and Kim 2012, and Huynh et al. 2015). A limitation of their studies was on setting the frequency band sensitive to the variation of the prestress forces. The effective frequency band was even over 800 kHz for a mono-tendon anchorage under compressive forcing about 100

[1)] Graduate Student
[2)] Professor

kN (Kim et al. 2010). To overcome the disadvantage, Nguyen and Kim (2012) developed an impedance-sensitive PZT interface technique which could reduce the frequency band to below 100 kHz and also the need of a high performance impedance analyzer. However, this design of PZT interface should be installed during the construction of the anchorage subsystem, so it is impossible to apply it into existing joint members. To monitor prestress-loss at existing tendon-anchorage systems with a predetermined frequency range, Huynh and Kim (2014) proposed a mountable PZT interface that could be mounted on (and detached from) the surface of bearing plates. By adopting the wireless sensor and the mountable PZT interface, the automated and cost-efficient operation can be implemented by embedded software for real applications (Koo et al. 2009). However, this fact also leads to an important issue that needs to be solved before real ambient applications. That is the performance of the mountable PZT interface under the temperature variation since boundary conditions and material constants of both sensor materials and host structures are temperature-dependent.

Researchers have worked on examining the effect of temperature variation on structural dynamic properties that are utilized for structural health monitoring (Kim et al. 2003, Ko and Ni 2005, Sohn 2007, Huynh et al. 2014). Temperature-driven variability of local impedance responses should also be quantified in the determination of impedance features that are used for damage monitoring (Park et al. 1999, Koo et al. 2009, and Hong et al. 2011, Yun et al. 2013). Park et al. (1999) presented that any changes in environmental temperature can lead to horizontal and vertical shifts of resonant impedance signatures. To remove the temperature effect from damage detection results, Park et al. (1999) used a modified root mean square deviation (RMSD) index based on the concept of effective frequency shift (EFS).

By employing the EFS concept, Koo et al. (2009) proposed a maximum cross-correlation (CC) index to minimize variations in impedance signatures due to temperature changes. An issue of the EFS-based technique is on selecting the frequency range which should be sensitive to damage but sufficiently narrow for the temperature compensation (Fabricio et al. 2014). Sepehry et al. (2011) and Yun et al. (2013) used artificial neural networks (ANNs) to compensate the temperature variation effect for impedance-based fault detection. However, the ANNs needs to be trained with multiple sets of measurements under varying temperatures for not only healthy but damaged scenarios. For existing structures, it is almost impossible to acquire training patterns of damaged states for the ANNs unless monitored structures are well-modeled by finite element (FE) impedance analysis. This study has been motived to monitor the prestress force in prestressed concrete (PSC) girders using the mountable PZT interface and to compensate the effect of temperature on prestress-loss monitoring results using the EFS-based technique.

2. IMPEDANCE-BASED PRESTRESS FORCE MONITORING AND EFS-BASED TEMPERATURE-EFFECT COMPENSATION TECHNIQUE

2.1 Impedance-based Prestress-Loss Monitoring using Mountable PZT Interface

The mountable PZT interface is designed to monitor EM impedance signatures of the prestressed tendon-anchorage system. As shown in Fig.1, the PZT interface is

mounted on the bearing plate that is subjected to the variation of the anchoring forces. In this study, the PZT interface is designed to deal with 1V-amplitude excitation and impedance monitoring using wireless sensor technology which offers an automated and cost-efficient monitoring systems (Lynch *et al.* 2006, Kim *et al.* 2014), and allows the frequency range of 10-100 kHz (Mascarenas *et al.* 2007). The mountable PZT interface has the fixed-fixed boundary condition by two outside contact bodies and the flexible beam section in the middle, as shown in Figs. 1 and 2. The PZT interface's structural properties are basically selected to fulfill the limitation of the wireless impedance monitoring.

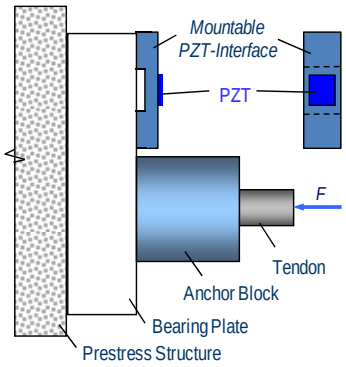

Fig. 1 Prestressed tendon-anchorage system with a mountable PZT interface

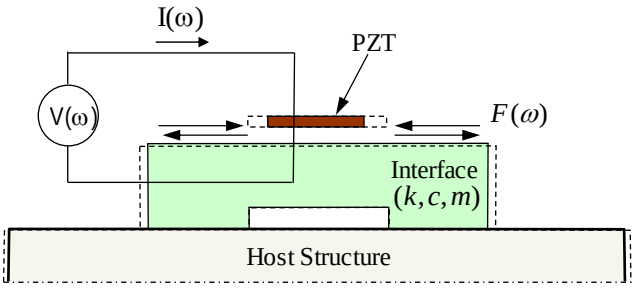

Fig. 2 PZT interface-structure model for SM impedance response

As shown in Fig. 2, the structural mechanical (SM) impedance response can be explained from the interaction between the PZT patch and the structure (e.g., the interface body). An input harmonic voltage $V(\omega)$ induces a deformation of the PZT due to the inverse piezoelectric effect. Then a force $F(\omega)$ against that deformation is induced into the structure (i.e., the interface body) and the PZT as well, because the PZT is surface-bonded to the interface structure. The SM impedance of the structure is defined as the ratio of force $F(\omega)$ to velocity $\dot{u}(\omega)$ as follows (Liang *et al*., 1994):

$$Z_s(\omega) = \frac{F(\omega)}{\dot{u}(\omega)} = c + m\frac{\omega^2 - \omega_n^2}{\omega} i \tag{1}$$

where c and m are the damping coefficient and the mass of the interfacing structure with the PZT patch, respectively; ω_n is the angular natural frequency of the interface structure; and ω is the angular frequency of the excitation voltage. The SM impedance is a function of structural properties (i.e., mass, damping, and stiffness), so that the change in structural parameters can be inversely interpreted by the change in the SM impedance

In practice, the electric current I(ω) is measured and then it is utilized to calculate electro-mechanical (EM) impedance as follows (Liang et al., 1994):

$$Z(\omega) = \frac{V}{I} = \left\{ i\omega \frac{w_a l_a}{t_a} \left[\hat{\varepsilon}_{33}^T - \frac{1}{Z_a(\omega)/Z_s(\omega) + 1} d_{3x}^2 \hat{Y}_{xx}^E \right] \right\}^{-1} \tag{2}$$

where $\hat{Y}_{xx}^{E} = (1+i\eta)Y_{xx}^{E}$ is the complex Young's modulus of the PZT patch at zero electric field; $\hat{\varepsilon}_{xx}^{T} = (1-i\delta)\varepsilon_{xx}^{T}$ is the complex dielectric constant at zero stress; d_{3x} is the piezoelectric coupling constant in x-direction at zero stress; and w_a, l_a, and t_a are the width, length, and thickness of the PZT patch, respectively. The parameters η and δ are structural damping loss factor and dielectric loss factor of piezoelectric material, respectively. Eq. (2) shows that the EM impedance, $Z(\omega)$, is a combining function of the SM impedance of the piezoelectric patch, $Z_a(\omega)$, and that of the host structure (e.g., the interface), $Z_s(\omega)$. The SM impedance is a function of mass, damping, and stiffness (i.e, stiffness is introduced from natural frequency, $k = m\omega_n^2$), as shown in Eq. (1). Thus, the change in structural parameters (m, k and c) caused by environmental conditions and damage can be represented by the change in the EM impedance.

For the 'PZT interface-bearing plate-anchor force' model, the change of the tendon-anchorage force may cause the change of the bearing plate's structural properties such as geometric and traction boundary conditions. Then, the change of the bearing plate's structural properties may cause the change of structural properties (i.e., geometrical and stress boundary conditions) of the PZT interface that is fixed on the surface boundary of the bearing plate. Consequently, impedance responses of the PZT interface are changed due to the change of the anchor force.

2.2 EFS-based Temperature-Effect Compensation Technique

Koo et al. (2009) utilized the concept of effective frequency shift (EFS) (Park et al. 1999) to develop a temperature-effect compensation method for minimizing false positive diagnoses. The EFS-based technique (Koo et al. 2009) has continued to be performed in recent damage detection jobs (Yun et al. 2013) since it requires simple computations and could be used for general impedance-based applications. The EFS-based temperature compensation technique is based on the effective frequency shift ($\delta\omega$) to give the maximum the correlation coefficient or the minimum correlation coefficient deviation (CCD) between the baseline impedance signature, $Z_o(\omega)$, and the current impedance signature after temperature change, $Z_1(\omega)$. The CCD index after the EFS (CCD_{EFS}) is calculated as follows:

$$CCD_{EFS} = \min_{\delta\omega}\left\{1 - \frac{E\left\{\left[\mathrm{Re}(Z_o(\omega_i)) - \mathrm{Re}(\bar{Z}_o)\right]\left[\mathrm{Re}(Z_1(\omega_i - \delta\omega)) - \mathrm{Re}(\bar{Z}_1)\right]\right\}}{\sigma_{Z_o}\sigma_{Z_1}}\right\} \tag{3}$$

in which E[.] is the expectation operation; $\mathrm{Re}(Z_o(\omega_i))$ and $\mathrm{Re}(Z_1(\omega_i))$ signifies the real parts of the EM impedances of the i^{th} frequency; $\mathrm{Re}(\bar{Z}_o)$ and $\mathrm{Re}(\bar{Z}_1)$ signifies the mean values of impedance signatures (real part); and σ_{Z_o} and σ_{Z_1} are the standard deviation values. A loop routine is performed until the value of the minimum CCD is obtained.

One of important issues of the EFS-based technique is on pre-determining the resonant frequency range which should be sensitive to structural changes for the damage detection and sufficiently narrow for the temperature compensation (Fabricio et al. 2014). A good match between the compensated impedance signature and the

baseline impedance signature could be obtained if the resonant peaks in the monitored frequency band exhibit approximately the same frequency shift. Ideally, the CCD index after the EFS is almost equal to 0 for undamaged scenarios under temperature variations, and larger than 0 if damage occurs. For alarming damage occurrence under uncertain conditions, the upper control limit (UCL) (Huynh and Kim 2014) is employed for the upper control limit of the CCD_{EFS} index. The occurrence of damage is indicated when the CCD_{EFS} index is larger than the UCL's value. Otherwise, there is no indication of damage occurrence.

4. EXPERIMENTS ON PSC GIRDER

4.1 Test-Setup of PSC Girder

Lab-scale experiments were conducted on a 6.4-meter PSC girder instrumented with a mountable PZT interface at tendon-anchorage, as shown in Fig. 3(a). The tested T-section girder was simply supported by the steel bars at both ends. The 28-day compressive strength of the concrete was 23.6 MPa, and the mass density was approximately 2400 kg/m^3. The PSC girder was eccentrically prestressed by a 7-wire straight tendon. The prestress forces were introduced into the tendon by a stressing jack as the tendon was anchored at one end and pulled out at the other. A load cell was installed at the left end to measure the applied prestress force. As shown in Fig. 3(b), an aluminum PZT Interface was designed and surface-bonded to the bearing plate of the right anchorage. For temperature measurement, a K-type thermocouple wire was setup on the top surface of the PSC girder.

The tendon was first pre-tensioned to 138.3 kN (14.1 ton) for the intact state. For each test, the PZT patch on the interface was excited by a harmonic excitation voltage with 1V-amplitude, and the impedance signature was measured by an impedance analyzer HIOKI 3532, as illustrated in Fig. 4(a). The impedance analyzer was set for automatically measuring every 10 minutes with the swept frequency within 10 ~ 55 kHz. A KYOWA (EDX-100A) data logger was used to monitor temperature via the K-type thermocouple wire, as shown in Fig. 4(b). The 1 Hz sampling rate was set for the temperature measurement system during the tests.

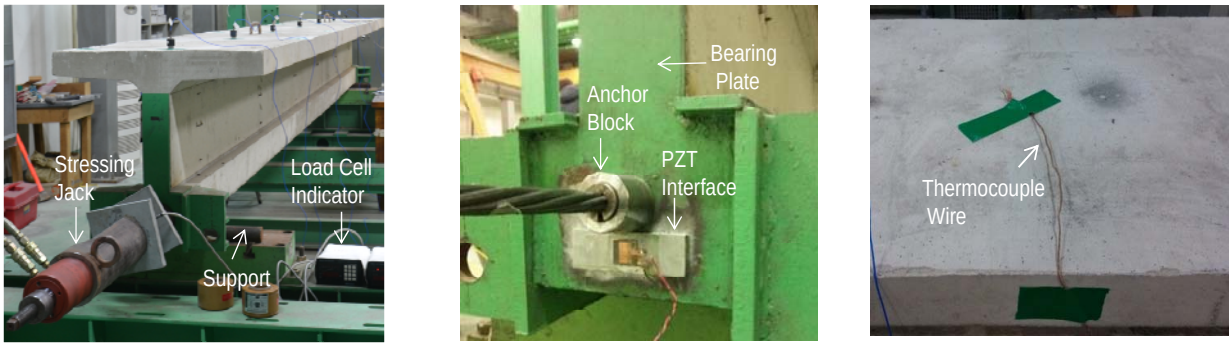

(a) PSC girder (b) Anchorage zone (c) Top of PSC girder

Fig. 3 Experimental setup in PSC girder

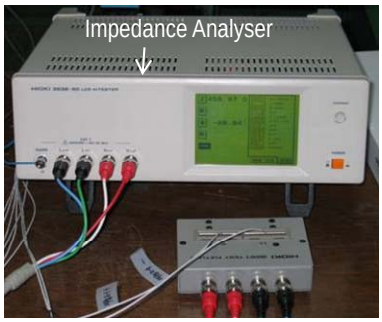

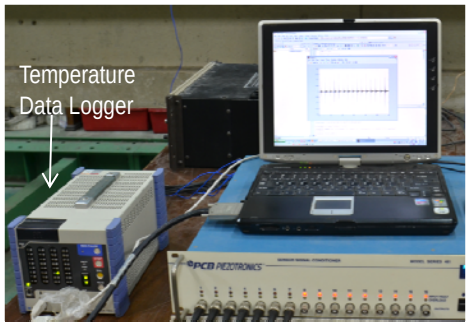

(a) Impedance analyzer HIOKI 3532 (b) A KYOWA temperature data logger

Fig. 4 Impedance and temperature measurement systems

4.2 Simulations of Temperature Variation and Prestress-Loss

Simulation of Temperature Variation As the first test scenario, the laboratory temperature was controlled to vary between 6.72°C to 22.33°C while the tendon force was set fixed as 138.3 kN. A series of tests were performed for 7 consecutive days from 28 January to 04 February, 2015 including 2 days for heating and 5 days for continuously auto-monitoring. The time history of the temperature variation simulated in the laboratory is shown in Fig. 5. At the beginning, the heaters were turn on to heat the underground laboratory temperature up as designed. The impedance tests started at 21:00 hour of January 29, 2015 as the laboratory temperature reached up to 22.33°C. Then the room temperature was controlled to decrease gradually by turning off the heaters for the remaining 5 days. It is noted that the room temperature changed day and night, as shown in Fig. 5. Totally, 669 measurement tests were performed on the PZT interface.

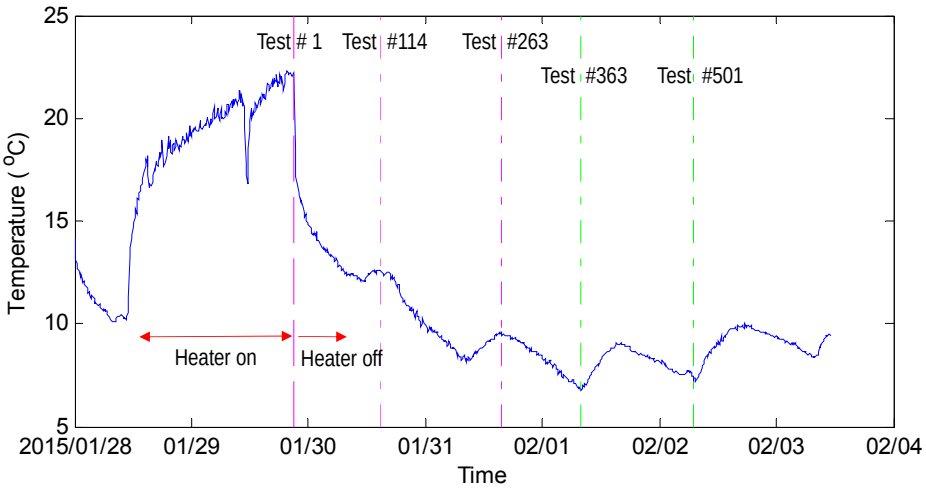

Fig. 5 Temperature history of temperature variation simulated in laboratory

Simulation of Prestress-Loss After the first test scenario, the impedance and temperature measurements were monitored continuously. As the second test scenario, the room temperature was then controlled by air conditioners in the laboratory. Figure 6 shows the time history of the measured temperature during the second test period on

04 January, 2015. As observed from the figure, the temperature variation was very small, about 1°C during the experimental tests. While the laboratory temperature was handled to almost constant of 19°C, a set of prestress-loss scenarios was simulated to the PSC girder from which the impedance responses of the PZT interface were measured for detecting the prestress-loss. Five prestressing levels: PS1 = 138.3 kN, PS2 = 128.5 kN, PS3 = 117.7 kN kN, PS4 = 108.9 kN, and PS5 = 99.1 kN were set for the test structure. By each prestressing levels, five sets of impedance data were sampled. Totally, 25 sets of impedance data were acquired from the PZT sensor.

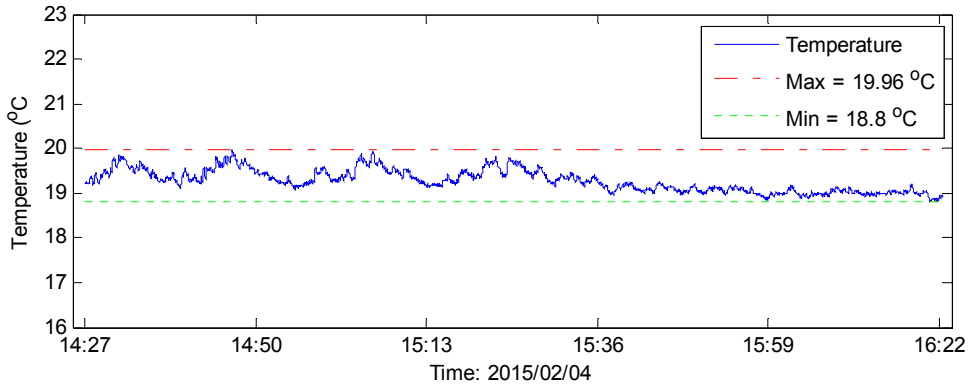

Fig. 6 Temperature history of unchanged temperature simulated in laboratory

5. FEASIBILITY OF MOUNTABLE PZT INTERFACE

To evaluate the performance of the mountable PZT interface-based prestress-loss monitoring in PSC girders, the impedance signatures measured during the prestress-loss simulation under constant temperature (i.e., the second test scenario) are used for computing damage indices.

5.1 Impedance Signatures under Prestress-Loss Scenarios

Fig. 7 shows real impedance signatures of the PZT interface in the wide frequency range 10 kHz - 55 kHz (901 interval points) for the healthy state PS1 and four damage cases PS2 ~ PS5 under constant temperatures. As compared to the impedance signatures of the same mountable PZT interface in the previous study (Huynh et al. 2015), the current impedance signatures have more resonant peaks when the PZT interface was implemented for the PSC girder. This implies that the contribution of the SM impedance to the EM impedance was considerable over this frequency range, as explained in Eq. (2). As observed in the figure, the all resonant peaks tended to sensitively shift left according to the decrement of prestress force. This indicates that modal stiffness of the whole anchorage was decreased with the prestress-loss of the PSC girder.

5.2 Prestress Force-Loss Monitoring Results

In impedance-based method, wide frequency bands containing many resonant peaks should be selected for the impedance-based damage detection (Park et al. 1999). Figure 8 shows the RMSD and CCD indices of the impedance signatures in the

frequency range 10-55 kHz computed for five prestressing levels (PS1 ~ PS5). It is worthy to note that the RMSD and CCD indices were the mean values obtained from five repeated measurements of each testing scenario. Both RMSD and CCD indices increased sensitively with the reduction of tendon force. As observed from Fig. 8, the RMSD and CCD indices of the wide frequency range 10-55 kHz show good indication of prestress-loss. It is also found that RMSD indices were higher than CCD indices for the considered frequency band. Therefore, the RMSD damage could be a better damage indicator for the impedance-based prestress force monitoring in PSC girders using mountable PZT interface. The experimental evaluation has proved the feasibility of the mountable PZT interface for the impedance monitoring of the prestress-loss in PSC girders under unchanged environmental conditions.

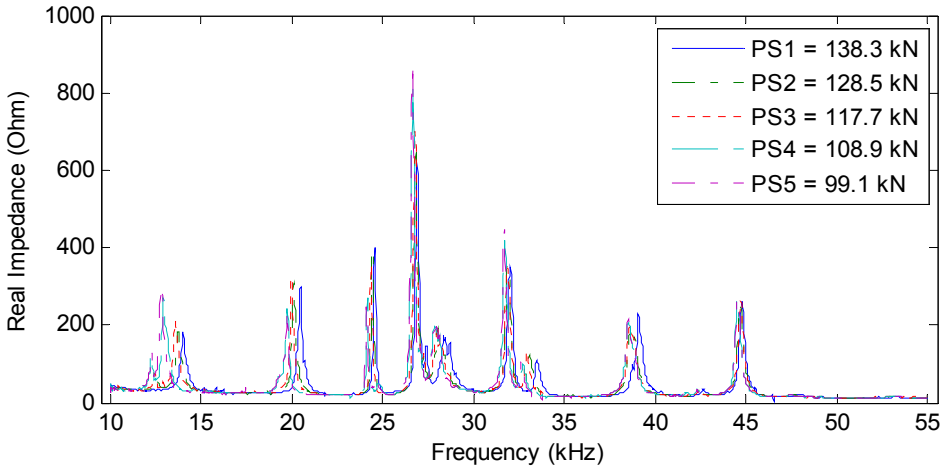

Fig. 7 Impedance signatures of PZT interface under various prestress forces

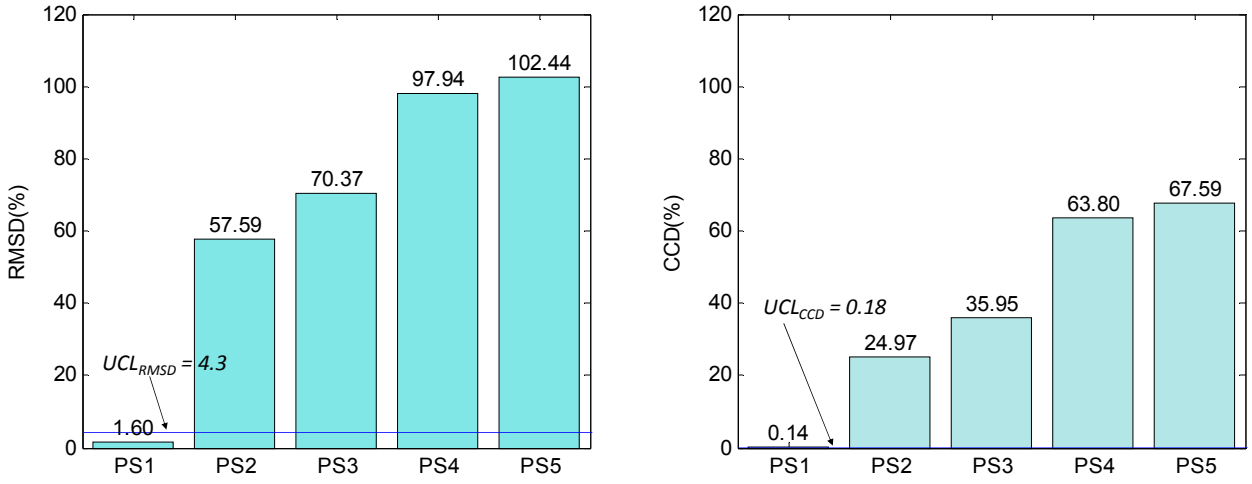

(a) RMSD index (b) CCD index

Fig. 8 Prestress force-loss monitoring results under constant temperatures

6. TEMPERATURE-EFFECT COMPENSATION USING EFS

6.1 Temperature-Effect on Impedance Signatures

As described earlier, the impedance signatures and temperature data were monitored continuously during the two test scenarios. For the temperature-effect compensation, the total number of impedance measurements is 689 including 669 for the intact state (i.e., the first test scenario) and 20 for the four prestress-loss states (i.e., the second test scenario). Figure 9 shows the 669 impedance measurements for the baseline (intact) state. The real impedance signatures were carried out for the frequency range 10-55 kHz under the temperature variation 6.72°C ~ 22.33°C. Within the frequency range of 10-55 kHz, several resonant peaks of the impedance signatures were taken into account, as shown in Fig. 10. It is observed that the temperature variation caused significant vertical and horizontal shifts of the impedance signatures. Therefore, the impedance monitoring using these impedance data could lead to false diagnostic results of the prestress-loss in the PSC girder. In the present work, the previously described EFS-based technique is used to compensate the temperature-effect on the impedance signatures measured from the anchorage of the PSC girder under the temperature variation (i.e., the first test scenario). Firstly, a frequency range used is selected among various frequency bands for the temperature compensation. Secondly, the PZT interface-based prestress-loss monitoring under temperature change is examined.

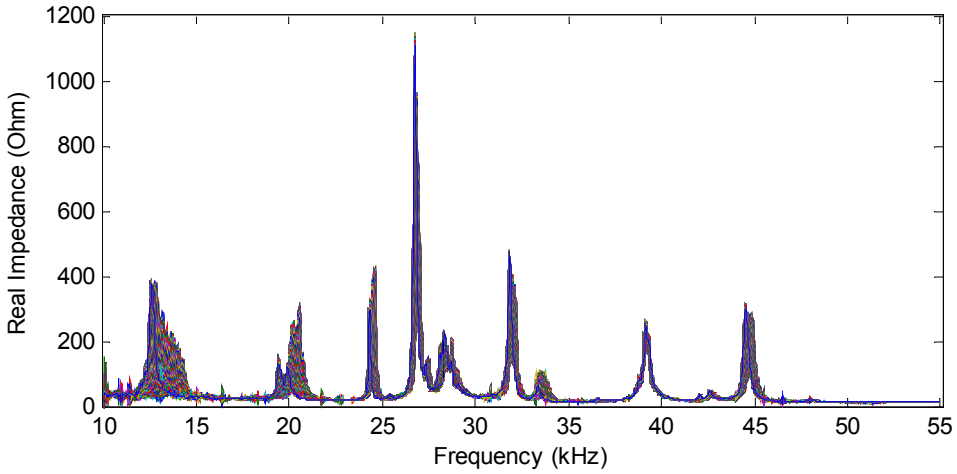

Fig. 9 Impedance signatures for frequency range 10-55 kHz measured from intact tendon-anchorage for temperatures: 6.72°C ~ 22.33°C

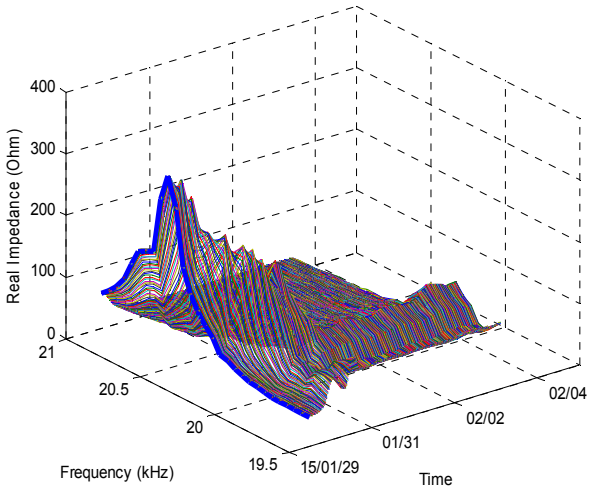

(a) Frequency range 19.5~21 kHz

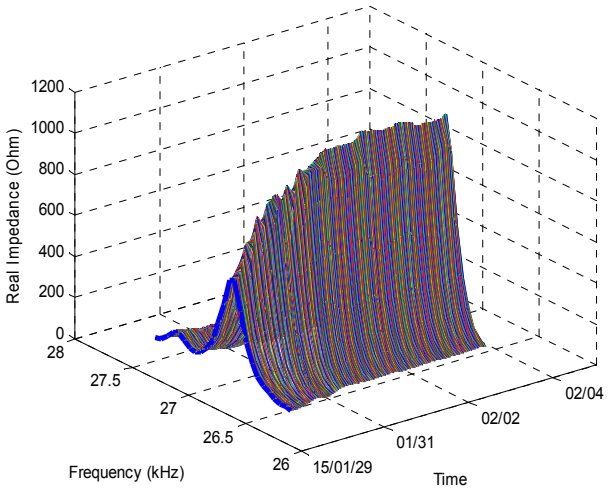

(b) Frequency range 26~28 kHz

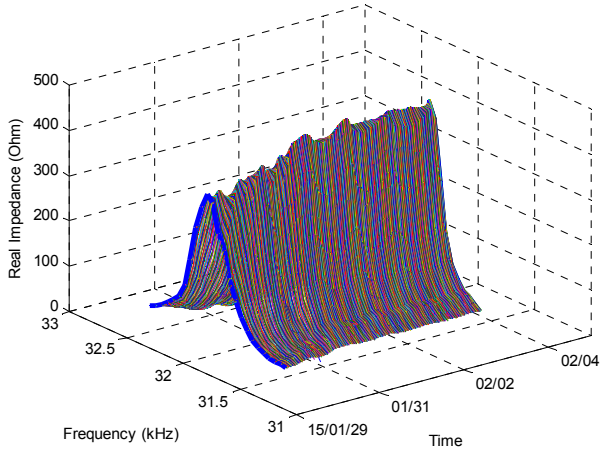

(c) Frequency range 31~33 kHz

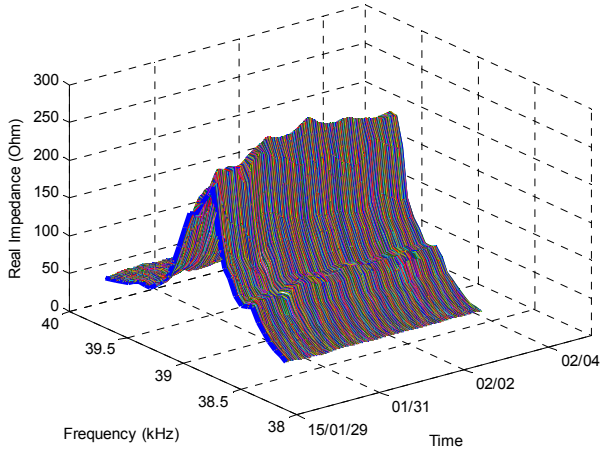

(d) Frequency range 38~40 kHz

Fig. 10 Time history of resonant peaks of impedance signatures measured from intact tendon-anchorage for temperatures: 6.72°C ~ 22.33°C

6.2 Frequency Ranges for Temperature Compensation

Figure 11 shows the 1st and the 114th impedance signatures in 12-47 kHz measured from the intact tendon-anchorage at 22.33°C and 12.63°C (about 10°C variation), respectively. Before EFS, a considerable CCD value, 37.8%, can be observed between two impedance signatures. After the EFS, however, the CCD value still remained significant, 16.7 %. Figure 12 shows the 114th and the 363th impedance signatures for the same frequency range measured at 12.63°C and 6.72°C (about 6°C variation), respectively. After EFS, the CCD value was reduced about half from 20.2% to 9.7%, but still considerable to be used for the baseline state. Figure 13 examined two close temperatures of two consecutive days: 6.72°C (363th test) and 7.19°C (501th test). As observed from the figure, the CCD value was remained the same as very small as 0.3% for before and after the EFS. Note that the real part of the impedance was used to calculate the CCD index.

In order to select a suitable frequency range for the temperature-effect compensation, several resonant ranges of the impedance signatures (for the intact

case) within 10-55 kHz were examined for calculating the CCD_{EFS} values. Figure 14 shows the CCD_{EFS} values for four examined frequency ranges: 12-47 kHz, 17-41 kHz, 23-35 kHz, and 25-35 kHz after the EFS. Note that the 1st impedance measurement at 22.33°C was selected as the reference for the calculation. For the four examined frequency bands, the CCD_{EFS} values obviously decreased as the temperature increased to 22.33°C. In other word, the correlation level between two impedance signatures increased when the temperature variation decreased. It is also observed that the wider frequency bands resulted in significant CCD_{EFS} values. This means the frequency band selected for the temperature compensation should be sufficiently narrow to void false diagnoses. From the analysis, the frequency range of 25-35 kHz can be selected for the temperature-effect compensation.

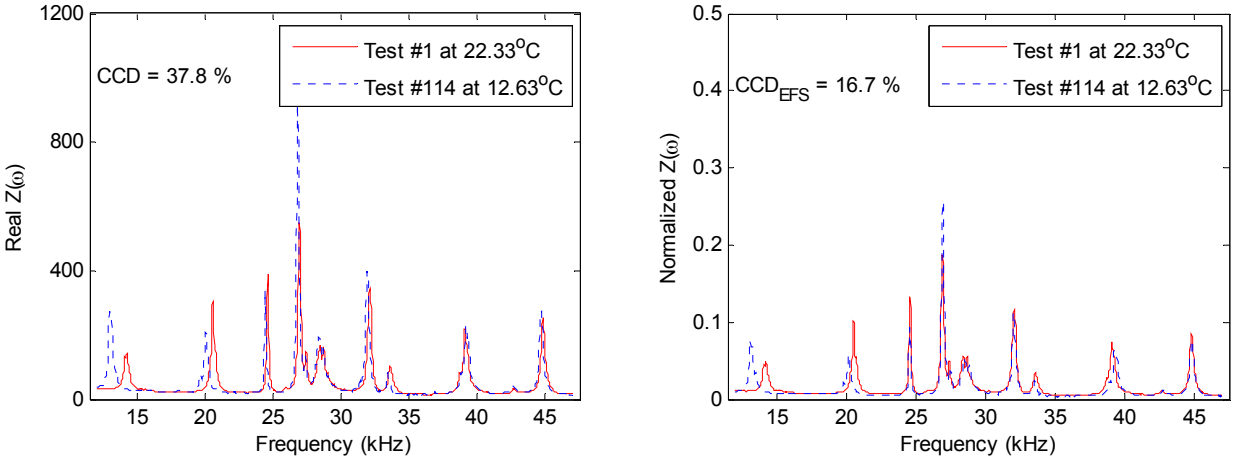

(a) Impedance before EFS (b) Normalized impedances after EFS

Fig. 11 Impedance signatures for frequency range 12-47 kHz measured from intact tendon-anchorage for two different temperatures: 22.3°C versus 12.63°C

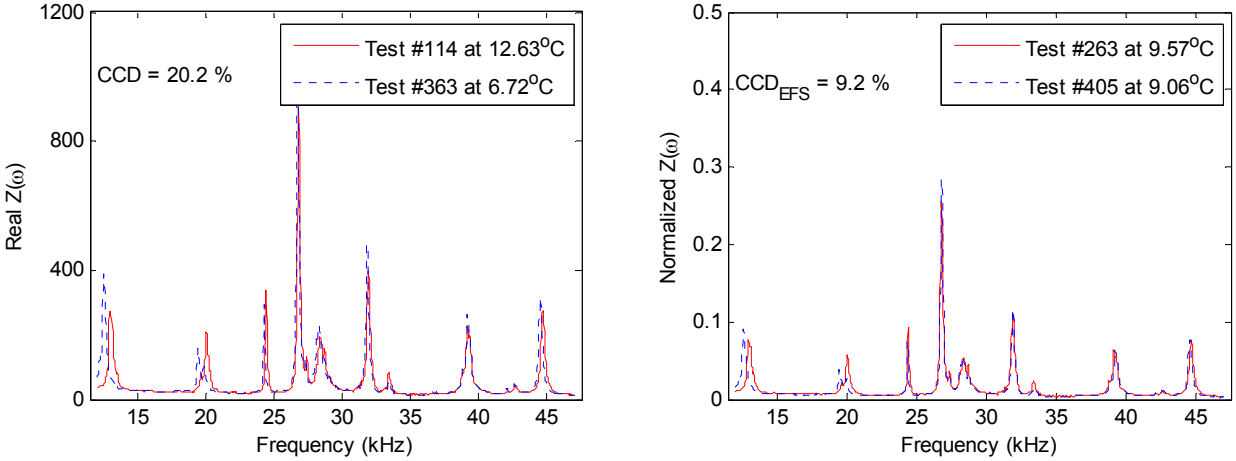

(a) Impedance before EFS (b) Normalized impedances after EFS

Fig. 12 Impedance signatures for frequency range 12-47 kHz measured from intact tendon-anchorage for two temperatures: 12.63°C versus 6.72°C

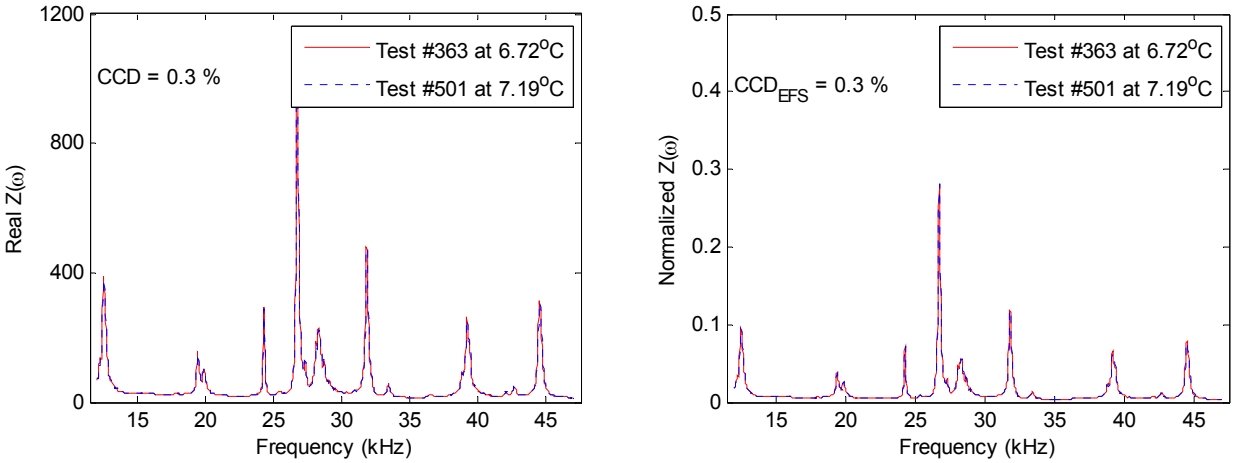

(a) Impedance before EFS (b) Normalized impedances after EFS

Fig. 13 Impedance signatures for frequency range 12-47 kHz measured from intact tendon-anchorage for two close temperatures: 6.72°C versus 7.16°C

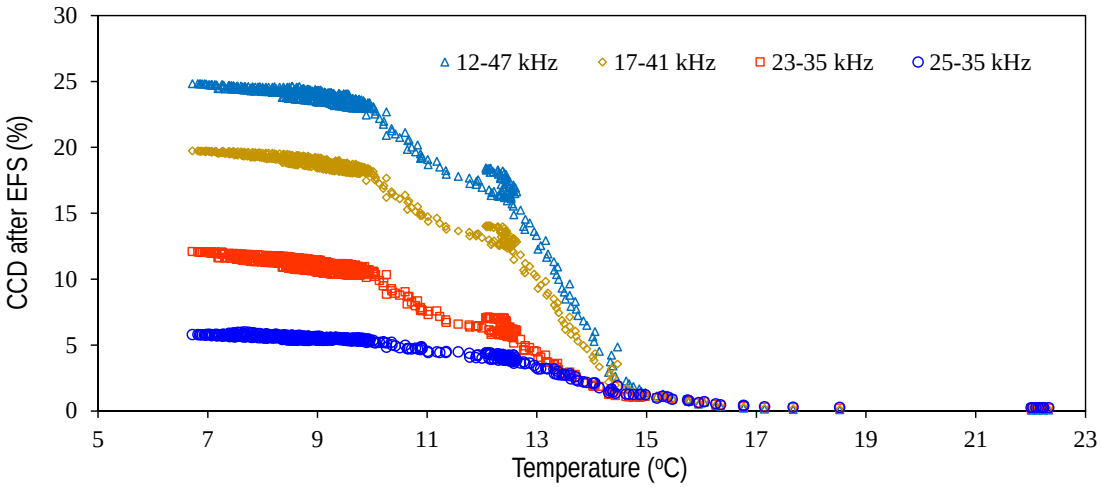

Fig. 14 CCD index after EFS for various frequency ranges of impedance signatures measured from intact tendon-anchorage for temperatures: 6.72°C ~ 22.33°C (Reference: Test #1 at 22.33°C)

Figure 15 shows the 1st and the 114th impedance signatures in 25-35 kHz measured from the intact tendon-anchorage at 22.33°C and 12.63°C, respectively. Before the EFS, a considerable CCD value, 30.1%, can be observed between two impedance signatures. After the EFS, however, the CCD value was significantly reduced to 3.9 %. Similarly, the CCD value between the 114th (at 12.63°C) and the 363th (at 6.72°C) impedance signatures was reduced from 11.6% to 1% after the EFS, as observed in Fig. 16. For two close temperatures of two consecutive days: 6.72°C (363th measurement) and 7.19°C (501th measurement), the CCD value was remained the same as very small as 0.4% for before and after the EFS, as shown in Fig. 17. It is found that excellent correlations between two impedance signatures over the frequency band 25-35 kHz were observed since the resonant peaks in this band exhibited mostly the same frequency shift.

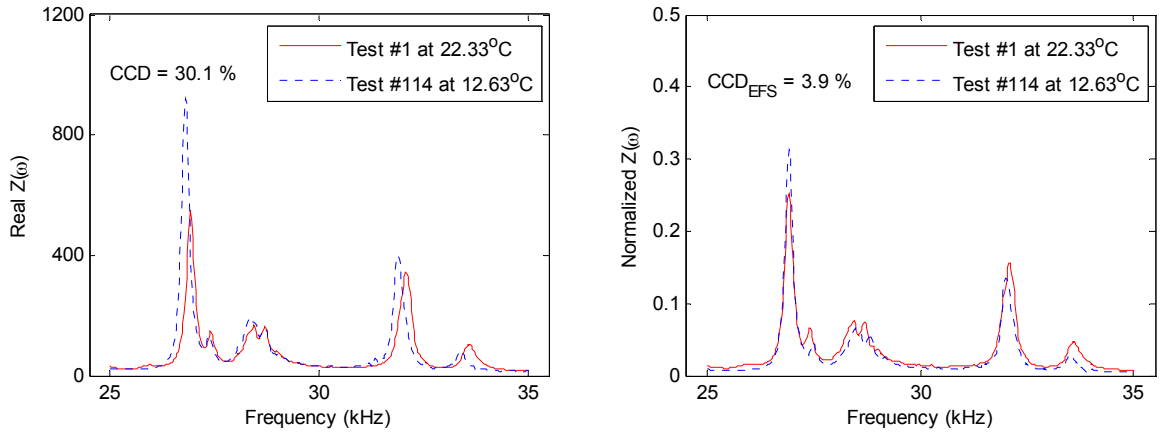

(a) Impedance before EFS (b) Normalized impedances after EFS

Fig. 15 Impedance signatures for frequency range 25-35 kHz measured from intact tendon-anchorage for two different temperatures: 22.3°C versus 12.63°C

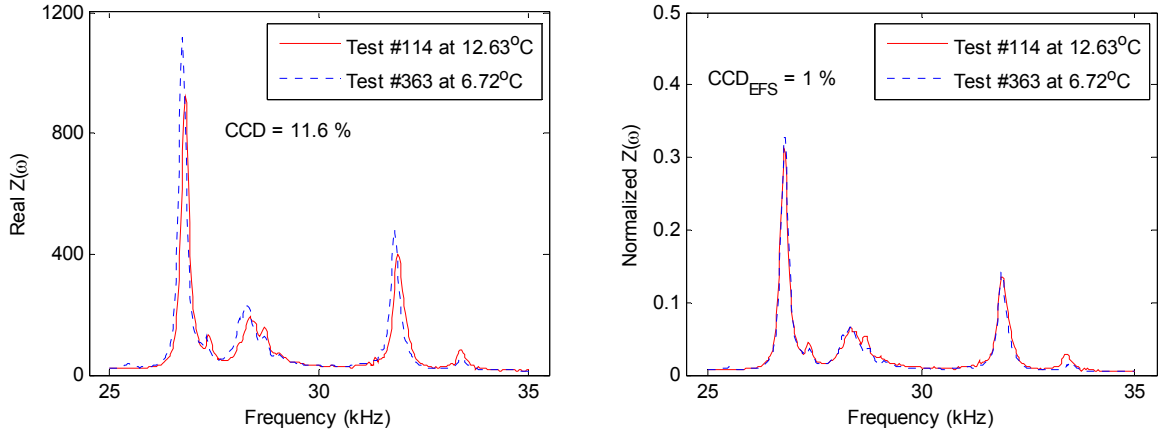

(a) Impedance before EFS (b) Normalized impedances after EFS

Fig. 16 Impedance signatures for frequency range 25-35 kHz measured from intact tendon-anchorage for two temperatures: 12.63°C versus 6.72°C

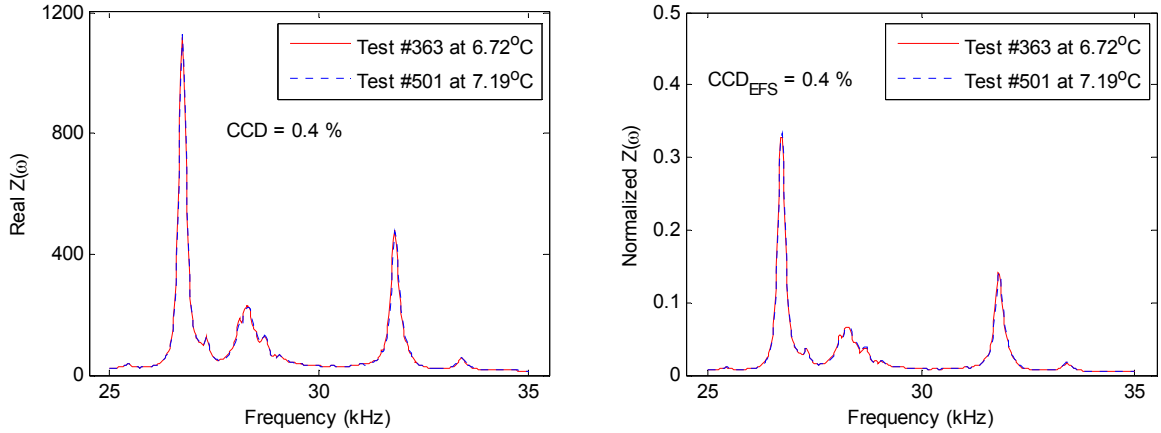

(a) Impedance before EFS (b) Normalized impedances after EFS

Fig. 17 Impedance signatures for frequency range 25-35 kHz measured from intact tendon-anchorage for two close temperatures: 6.72°C versus 7.16°C

6.3 Prestress-Loss Monitoring under Temperature Variation

Next, the CCD_{EFS} index was calculated for the 689 impedance measurements measured during the temperature variation and prestress-loss events. Note that in the EFS-based temperature compensation technique, the impedance signature measured at approximately the mean temperature of the temperature variation is usually selected as the baseline impedance (Koo et al. 2009). Therefore, the 114th impedance measurement at 12.63^{o}C was set as the reference impedance for the calculation.

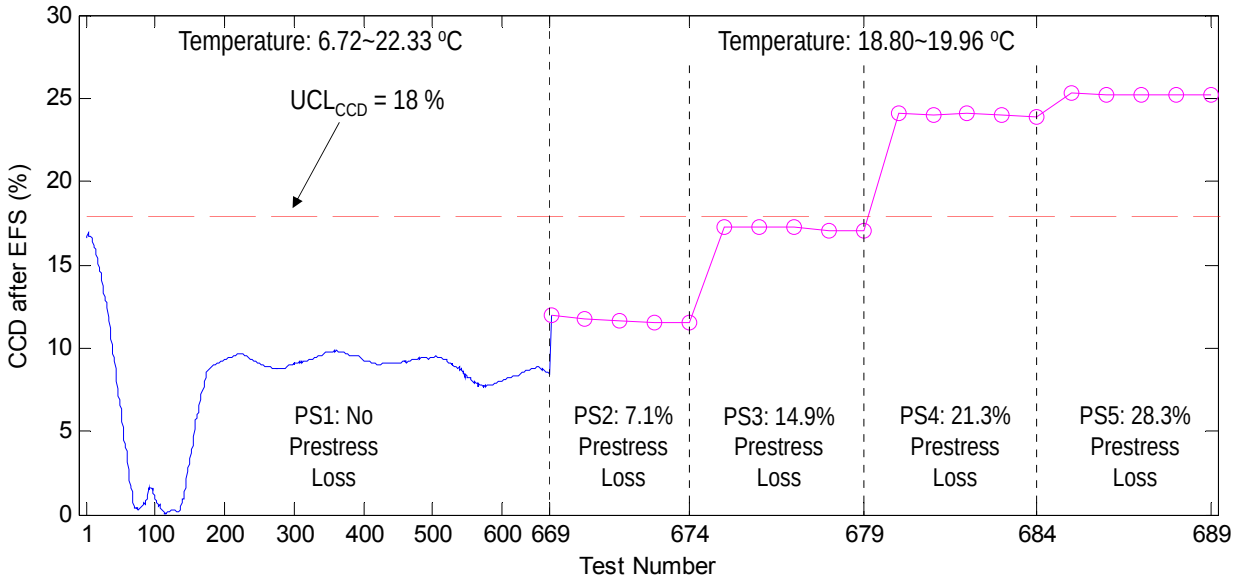

(b) Frequency ranges 12-47 kHz

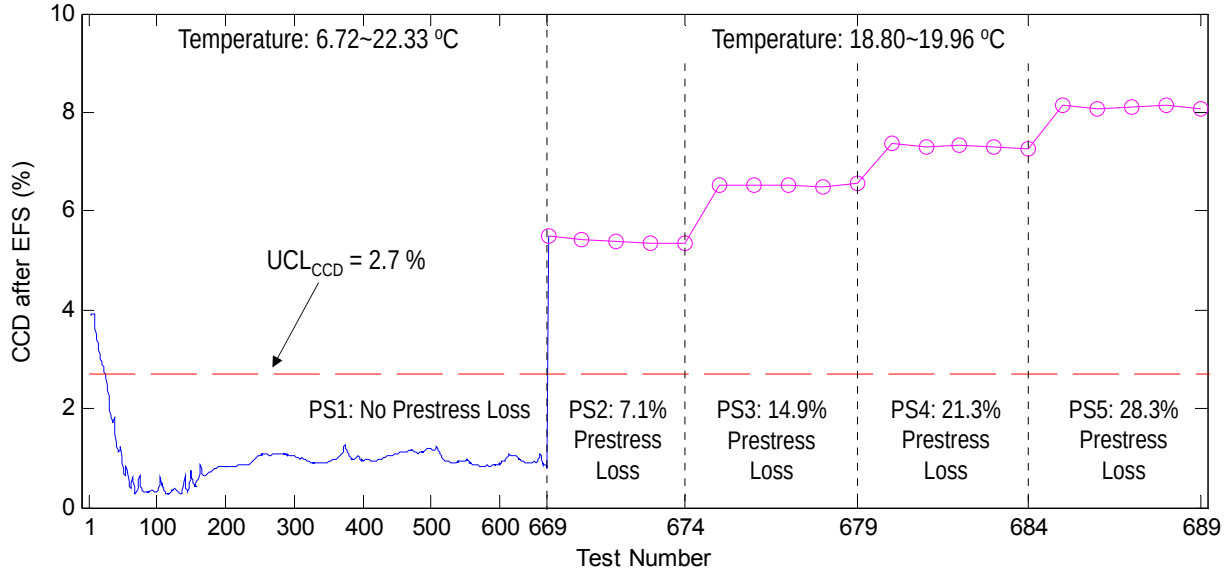

(b) Frequency ranges 25-35 kHz

Fig. 18 Prestress-loss monitoring results under temperature variation using CCD_{EFS} index of impedance signatures (Reference: Test #114 at 12.63^{o}C)

The prestress-loss monitoring results using the CCD_{EFS} index (after the EFS) computed over the wide frequency range of 12-47 kHz, and the selected frequency range of 25-35 kHz are shown in Figure 18. It is found that the CCD_{EFS} values increased with the increment of the prestress-loss. When the frequency range of 12-47 kHz was employed, the UCL of the CCD_{EFS} was significant as 18%, as shown in Fig. 18(a). It is observed from the figure that the mountable PZT interface was failed to detect the second and the third prestressing levels (PS2~PS3) of the PSC girder, only successfully alarmed when the prestress-loss increased up to 21.3 % (PS4). When the frequency range of 25-35 kHz was used, however, the UCL of the CCD_{EFS} index was significantly decreased to 2.7% and the CCD_{EFS} values jumped over the upper control limit even for the small prestress-loss level of 7.1% (PS2), as shown in Fig. 18(b). This means that the mountable PZT interface successfully detected the prestress-loss in the PSC girder under the temperature change.

7. CONCLUSION

From the analyses of prestress-loss monitoring in the PSC girder, the following conclusions have been made: (1) the prestress-loss events in the PSC girder under constant temperatures were successfully detected by implementing the mountable PZT interface at the tendon-anchorage; (2) when the PZT interface was installed at the tendon-anchorage of the PSC girder, there existed more resonant peaks in impedance signatures than the previous observations for the same PZT interface (Huynh et al. 2015); (3) for the temperature-effect compensation using the EFS-based technique, the wider frequency range was selected the lower correlation level between impedance measurements was observed; (4) a selecting process should be pre-performed to select a suitable frequency range for the EFS-based temperature-effect compensation; (5) the mountable PZT interface successfully detected the prestress-loss in the PSC girder under the temperature variation.

ACKNOWLEDGEMENT

This work was supported by Basic Science Research Program through the National Research Foundation of Korea (NRF) funded by the Ministry of Education, Science and Technology (NFR-2013R1A1A2A10012040). Graduate student involved in this research were also supported by the Brain Korea 21 Plus program of Korean Government.

REFERENCES

Fabricio G. B., Danilo E. B., Vinicius A. D. A.,and Jose A. C. U. (2014), “An experimental study on the effect of temperature on piezoelectric sensors for impedance-based structural health monitoring”, *Sensors 2014*, **14**, 1208-1227

Huynh, T.C. and Kim, J.T. (2014), “Impedance-based cable force monitoring in tendon-anchorage using portable PZT-interface technique”, *Math. Probl. Eng.*, **2014**, Article ID 784731, 11 pages.

Huynh, T.C., Park, Y.H., Park, J.H., Hong, D.S., and Kim, J.T. (2014), "Effect of temperature variation on vibration monitoring of prestressed concrete structures", *Shock and Vibration*, Article ID 741618.

Huynh, T.C., Lee, K.S., and Kim, J.T. (2015), "Local dynamic characteristics of PZT impedance interface on tendon anchorage under prestress force variation", *Smart Structures and Systems*, **15**(2), 375-393.

Ko, J.M. and Ni, Y.Q. (2005), "Technology developments in structural health monitoring of large-scale bridges", *Eng. Struct.*, **27**, 1715-1725.

Koo, K.Y, Lee, J.J., Yun, C.B., and Kim, J.T. (2009), "Damage detection in beam-like structures using deformations obtained by modal flexibilities matrices", *Advances in Science and Technology*, **56**, 483-488.

Kim, J.T., Huynh, T.C. and Lee, S.Y. (2014), "Wireless structural health monitoring of stay cables under two consecutive typhoons", *Struct. Monit. Maint.,* **1**(1), 47-67.

Kim, J.T., Na, W.B., Park, J.H. and Hong, D.S. (2006), "Hybrid health monitoring of structural joints using modal parameters and EMI signatures", *Proceeding of SPIE*, San Diego, USA.

Kim, J.T., Park, J.H., Hong, D.S. and Park, W.S. (2010), "Hybrid health monitoring of prestressed concrete girder bridges by sequential vibration-impedance approaches", *Engineering Structures*, **32**, 115-128.

Kim, J.T., Yun, C.B. and Yi, J.H. (2003), "Temperature effects on frequency-based damage detection in plate-girder bridges", *J. KSCE*, **7**(6), 725-733.

Liang, C., Sun, F.P. and Rogers, C.A. (1994), "Coupled electro-mechanical analysis of adaptive material - Determination of the actuator power consumption and system energy transfer", *J. Intel. Mat. Syst. Str.*, **5**, 12-20.

Lynch, J.P., Wang, W., Loh, K.J., Yi, J.H. and Yun, C.B. (2006), "Performance monitoring of the Geumdang Bridge using a dense network of high-resolution wireless sensors", *Smart Mat.Struct.*, **15**(6), 1561-1575.

Mascarenas, D.L., Todd, M.D., Park, G. and Farrar, C.R. (2007), "Development of an impedance-based wireless sensor node for structural health monitoring", *Smart Materials and Structures*, **16**(6), 2137-2145.

Nguyen, K. D. and Kim, J. T. (2012), "Smart PZT-interface for wireless impedance-based prestress-loss monitoring in tendon-anchorage connection," *Smart Structures and Systems*, **9**(6), pp. 489–504.

Park, G.; Kabeya, K.; Cudney, H.; Inman, D. (1999), Impedance-based structural health monitoring for temperature varying applications. *JSME Int. J. Ser. A Solid Mech. Mater. Eng*, **42**, 249–258.

Sepehry, N., Shamshirsaz, M., and F. Abdollahi (2011),"Temperature Variation Effect Compensation in Impedance-Based Structural Health Monitoring Using Neural Networks", *Journal for Intelligent Material Systems and Structures*, **20**(10), 1-8

Sohn, H. (2007) "Effects of environmental and operational variability on structural health monitoring", *Philosophical Transactions of the Royal Society A*, **365**, 539-560.

Yun, C.; Cho, S.; Park, H.; Min, J.; Park, J. (2013), "Smart wireless sensing and assessment for civil infrastructure", *Struct. Infrastruct. Eng. Maint. Manag. Life-Cycle Design Perform.* doi:10.1080/15732479.2013.769011.